International Symposium
On Turbulence and Shear Flow
Phenomena (TSFP-9)
June 30 - July 3, 2015 *Melbourne, Australia*

APPROXIMATION OF THE EXACT TRAVELING WAVE SOLUTIONS IN WALL-BOUNDED FLOWS USING RESOLVENT MODES

Rashad Moarref
Graduate Aerospace Laboratories
California Institute of Technology
1200 E California Blvd, Pasadena, CA 91125, USA
rashad@caltech.edu

Jae Sung Park
Chemical and Biological Engineering
University of Wisconsin-Madison
1415 Engineering Dr, Madison, WI 53706, USA
park329@wisc.edu

Ati S. Sharma
Engineering and the Environment
University of Southampton
22 University Rd, Southampton, SO17 1BJ, UK
a.sharma@soton.ac.uk

Ashley P. Willis
School of Mathematics and Statistics
University of Sheffield
Hicks Building, Hounsfield Rd, Sheffield, S3 7RH, UK
a.p.willis@sheffield.ac.uk

Michael D. Graham
Chemical and Biological Engineering
University of Wisconsin-Madison
1415 Engineering Dr, Madison, WI 53706, USA
graham@engr.wisc.edu

Beverley J. McKeon
Graduate Aerospace Laboratories
California Institute of Technology
1200 E California Blvd, Pasadena, CA 91125, USA
mckeon@caltech.edu

ABSTRACT

Over the past decade, significant attention has been devoted to computing and understanding the exact traveling wave solutions (TWS) of the Navier-Stokes equations (NSE). To better understand the linear and nonlinear mechanisms in the TWS, we consider a low-order approximation of the TWS in terms of a weighted sum of resolvent modes. The resolvent modes represent the most amplified forcing and response modes by the linear mechanisms in the NSE and the weights represent the scaling influence of the nonlinear terms. We show that only a few resolvent modes are sufficient to capture most of the dynamics of the TWS in channel and pipe flows. For the most energetic Fourier modes in the wall-parallel directions, it is shown that the first few most amplified resolvent modes capture approximately 90% of the energy of the velocity field. This illustrates the integral role of linear amplification mechanisms in the NSE in shaping the wall-normal profile of the response. In addition, we show that approximately less than 30% of the nonlinear terms in the NSE is captured by the corresponding resolvent forcing modes. Therefore, a relatively small portion of the Reynolds-stress gradient is required for sustaining the velocity fluctuations.

INTRODUCTION

Wall-bounded turbulent flows are dominated by coherent structures which motivates the search for their low-order decomposition and modeling. The exact TWS (e.g. Waleffe (2001, 2003); Wedin & Kerswell (2004); Li *et al.* (2006); Willis & Kerswell (2008); Pringle *et al.* (2009)) of the NSE represent attractive benchmarks for studying low-order models of wall turbulence. This is because (i) the TWS can be interpreted as state-space skeleton of turbulence, some of which represent the edge states, i.e. small perturbations around them drive the flow to either laminar or turbulent states; and (ii) the TWS contain only one wavespeed (the ratio between temporal frequency and streamwise wavenumber of the fluctuations) and thus, they are simpler solutions to the NSE relative to the full turbulent flow.

Sharma *et al.* (2015) used a gain-based decomposition of the TWS in terms of a weighted sum of resolvent modes (McKeon & Sharma, 2010) to show the low-rank nature of representative families of TWS in both pipes and channels, see figure 1. The pipe solutions were generated by continuation to the bulk Reynolds number $Re_B = 5300$ (friction Reynolds number $Re_\tau = 106 - 214$) from the solutions of Pringle *et al.* (2009) using *openpipeflow.org*. They are classified into solutions that have mirror, shift-and-reflect and rotational symmetries (N-class) and solutions that have only shift-and-reflect symmetry (S-class). The channel solutions were generated using the code *channelflow* (Gibson *et al.*, 2008). The P1 (at $Re_\tau = 75$) and P3 (at $Re_\tau = 85$) families are active in the core of the channel, and approach the laminar flow as Re_τ increases. The P4 solutions (at $Re_\tau = 85$) are highly nonlinear with fluctuations localized near the critical layer. At high Reynolds numbers, the importance of the critical layer mechanism becomes clearer (e.g. Viswanath (2009); Hall & Sherwin (2010); Deguchi & Hall (2014)). When applicable, the high-drag (upper-branch) and low-drag (lower-branch) solutions are respectively denoted by 'U' and 'B'.

The resolvent modes represent the most amplified forc-

ing and response modes by the linear mechanisms in the NSE and the weights represent the scaling influence of the nonlinear terms. For channel and pipe flows at the stationary steady state, the resolvent modes are independently determined for each wall-parallel wavenumber pair and temporal frequency. In addition, the resolvent modes are known to admit Reynolds-number scaling (Moarref *et al.*, 2013). Computing the weights is more challenging since they depend on the nonlinear interaction of the resolvent modes. A brief overview of the resolvent formulation in channel flow is provided next. The velocity field $\mathbf{u}(x,y,z,t)$ is decomposed into Fourier modes $\hat{\mathbf{u}}(y,\kappa,\omega)$ in the homogeneous directions and time. Here, $\boldsymbol{\kappa} = [\kappa_x \ \kappa_z]$ is the wavenumber vector, κ_x and κ_z are the streamwise and spanwise wavenumbers, and ω is the temporal frequency. The NSE for the fluctuations around the mean velocity $\mathbf{U}$ are given by

$$\begin{aligned} -\mathrm{i}\omega\hat{\mathbf{u}} + (\mathbf{U}\cdot\nabla)\hat{\mathbf{u}} + (\hat{\mathbf{u}}\cdot\nabla)\mathbf{U} + \nabla\hat{p} - (1/Re_\tau)\Delta\hat{\mathbf{u}} &= \hat{\mathbf{f}} \\ \nabla\cdot\hat{\mathbf{u}} &= 0 \end{aligned} \tag{1}$$

where p is the pressure, $\mathbf{f} = -(\mathbf{u}\cdot\nabla)\mathbf{u}$ is considered as a forcing term that drives the fluctuations, $\nabla = [\mathrm{i}\kappa_x \ \partial_y \ \mathrm{i}\kappa_z]^T$, and $\Delta = \partial_{yy} - \kappa_x^2 - \kappa_z^2$. The input-output relationship between $\hat{\mathbf{f}}$ and $\hat{\mathbf{u}}$ is governed by the resolvent operator H

$$\hat{\mathbf{u}}(y,\kappa,\omega) = H(\kappa,\omega)\hat{\mathbf{f}}(y,\kappa,\omega) \tag{2}$$

For any (κ,ω), a complete basis in y is determined using the singular value decomposition of H. This decomposition yields a set of forcing $\hat{\phi}_j$ and response $\hat{\psi}_j$ resolvent modes that are ordered by the gain σ_j. For the Reynolds-stress gradient $\hat{\mathbf{f}}$ in the direction of the forcing mode $\hat{\phi}_j$, the velocity $\hat{\mathbf{u}}$ will be in the direction of the response mode $\hat{\psi}_j$ and amplified by the gain σ_j. Here, $\hat{\psi}_j$ and $\hat{\phi}_j$ are the left and right resolvent modes. Each resolvent mode is a propagating wave with streamwise speed $c = \omega/\kappa_x$. Owing to the integral role of c in the wall-normal localization[5] and scaling[6] of the resolvent modes, it is advantageous to parameterize the modes by c instead of ω.

Using N resolvent modes, the velocity and forcing fields are approximated as

$$\begin{aligned} \hat{\mathbf{u}}(y,\kappa,c) &= \sum_{j=1}^{N} \chi_j(\kappa,c)\,\sigma_j(\kappa,c)\,\hat{\psi}_j(y,\kappa,c) \\ \hat{\mathbf{f}}(y,\kappa,c) &= \sum_{j=1}^{N} \chi_j(\kappa,c)\,\hat{\phi}_j(y,\kappa,c) \end{aligned} \tag{3}$$

where the weights χ_j denote the projection of $\hat{\mathbf{f}}$ onto $\hat{\phi}_j$. Since $\mathbf{f}$ is quadratic in $\mathbf{u}$, the modes that directly interact constitute triads whose weights are coupled via the interaction coefficients $\mathscr{N}_{lij}$ (McKeon *et al.*, 2013)

$$\chi_l(\kappa,c) = \sum_{i,j=1}^{N} \int \mathscr{N}_{lij}(\kappa,\kappa',c)\,\chi_i(\kappa',c)\,\chi_j(\kappa-\kappa',c)\,\mathrm{d}\kappa' \tag{4}$$

The explicit computation of the weights requires projecting the NSE onto the known resolvent modes and solving the resulting equations. In the present work, the weights are determined by projecting the known velocity field from numerically-computed TWS onto the resolvent modes.

class	κ_x	Re_τ	$c/2U_B$
S1	0.78	106	0.81
S1	0.34	107	0.78
S2b	1.24	107	0.76
S2b	0.95	108	0.76
S2b	0.39	110	0.71
S2b	0.24	122	0.62
N2L	1.73	109	0.83
N2L	1.24	109	0.82
N2L	0.55	111	0.78
N2L	0.15	117	0.70
N3L	1.25	111	0.74
N4L	1.70	114	0.69
N2U	1.25	151	0.66
N2U	1.01	156	0.66
N2U	0.80	177	0.64
N4U	1.70	214	0.55
class	Re_B	Re_τ	$c/2U_B$
P1L	3200	75	0.58
P3L	4533	85	0.52
P4L	3677	85	0.58
P1U	2267	75	0.49
P3U	1733	85	0.35
P4U	2200	85	0.55

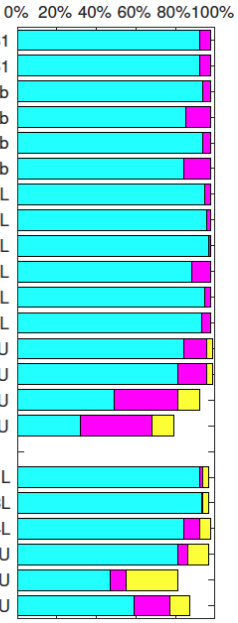

Figure 1. *Left:* All invariant solutions considered in this study, covering a range of solution classes, Re_τ and wavespeeds c. The upper set refer to the pipe solutions, the lower set to the channel solutions. All the pipe solutions are at $Re_B = 5300$, and U_B denotes the bulk velocity. *Right:* Fraction of energy captured by a projection of $1,5,10$ model modes (pipe) or $1,2,5$ model mode pairs (channel) per Fourier mode, for all studied solutions. Figures reproduced from Sharma *et al.* (2015).

APPROXIMATING TWS USING RESOLVENT MODES

We apply Fourier transform to the velocity field from numerically-computed exact TWS and project the Fourier modes onto the resolvent modes that are parameterized by the (κ_x, κ_z, c) triplet. Since the TWS contain a single speed c, only the resolvent modes with that speed are considered. Ten most amplified resolvent modes per Fourier wavenumbers are considered to compute the correct weights. The nonlinear term is reconstructed using the correctly-weighted resolvent forcing modes and compared with the actual nonlinear term from simulations.

An overview of the pipe and channel results from Sharma *et al.* (2015) is presented first. The efficacy of the resolvent modes in capturing the velocity fluctuations of the TWS is summarized in figure 1. We note that the fluctuations' kinetic energy is well-captured by the most amplified resolvent modes. For example, the most amplified mode pair captures 84% and 59% of the fluctuations' energy in the P4L and P4U solutions, respectively. These numbers are respectively 98% and 87% for the five most amplified mode pairs. The low-order approximation of representative TWS in pipes and channels is further illustrated in figures 2 and 3.

In the rest of the paper, we pay special attention to the upper and lower branches of the P4 solutions; similar results are shown in the pipe flow. Park & Graham (2015) showed that the mean velocities of P4U and P4L are similar to the von Kármán and Virk profiles, respectively. In addition, the

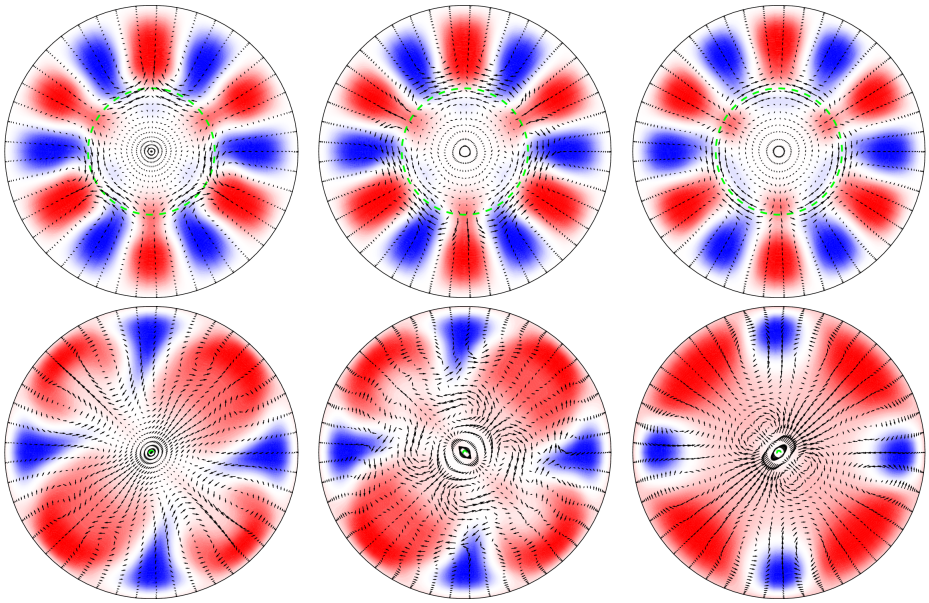

Figure 2. The captured velocity fluctuations in the N3L solution (top row) and the N2U solution (bottom row) in a pipe. From left to right: actual solution; projection onto the five most amplified model modes pairs per Fourier wavenumbers, projection onto the most amplified model mode pair per Fourier wavenumbers. Figures reproduced from Sharma *et al.* (2015).

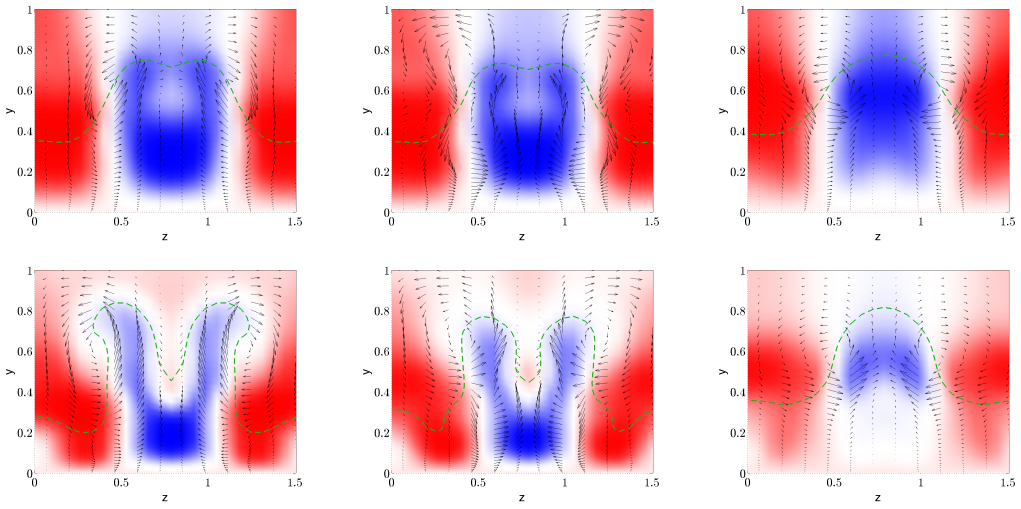

Figure 3. The captured velocity fluctuations (lower half shown) in the P4L solution (top row) with $Re_\tau = 85$ and $c = 25u_\tau$ and the P4U solution (bottom row) with $Re_\tau = 85$ and $c = 14.2u_\tau$. From left to right: actual solution; projection onto the five most amplified model modes pairs per Fourier wavenumbers, projection onto the most amplified model mode pair per Fourier wavenumbers.

normal or 'active' turbulent trajectory lies within a region close to the P4U solution while the turbulent trajectory occasionally escapes from this region and approaches the P4L solution. The P4 family is computed in a periodic channel of size $L_x = \pi h$ and $L_z = \pi h/2$ (h is the channel half-width). The wavespeed c is $25u_\tau$ in P4L and $14.2u_\tau$ in P4U where u_τ is the friction velocity.

Figure 4 summarizes the projection of the velocity fluctuations and the nonlinear term in the NSE (the Reynolds-stress gradient) onto the resolvent modes for the P4L solution. Only the Fourier modes that contain more than 1% of the turbulent kinetic energy are shown and the corresponding wall-parallel wavenumbers are indicated. Notice that κ_x and κ_z are normalized with $1/h$. Figure 4(a) shows that the mode with $\kappa_x = 0$ and $\kappa_z = 4$ (corresponding to the spanwise wavelength $\lambda_z = L_z$) dominates the velocity field. On the other hand, figure 4(b) reveals that the norm of the nonlinear terms is largest for $\kappa_x = 2$ (corresponding to the streamwise wavelength $\lambda_x = L_x$) and $\kappa_z = 0$.

The energy percentage of the Fourier modes that is captured by the first to fifth pairs of the most amplified resolvent modes is shown in figure 4(c). Approximately 96% of the dominant Fourier mode ($\kappa_x = 0$, $\kappa_z = 4$) is contained in the first mode pair, and 99% of the second dominant mode

($\kappa_x = 0,\ \kappa_z = 12$) is contained in the first two pairs of resolvent modes. Capturing 95% of the dominant spanwise-constant mode ($\kappa_x = 2,\ \kappa_z = 0$) requires the first five pairs of resolvent modes.

Figure 4(d) shows the projection of the nonlinear terms in the P4L solution onto the forcing modes. Notice that a relatively small portion of the nonlinear terms is necessary for sustaining the fluctuations. For example, 96% of the dominant mode ($\kappa_x = 0,\ \kappa_z = 4$) is forced by approximately 6% of the Reynolds-stress gradient at this wavenumber pair. Capturing the remaining 4% of the kinetic energy adds 38% to the forcing energy (corresponding to the second to fifth pairs of resolvent modes). In addition, the second ($\kappa_x = 0$, $\kappa_z = 12$) and third ($\kappa_x = 0,\ \kappa_z = 8$) dominant modes require less than 20% of the Reynolds-stress gradient $\mathbf{u} \cdot \nabla \mathbf{u}$. Note also that the dominant forcing mode (see $\kappa_x = 2$ and $\kappa_z = 0$) results in a small contribution to the total fluctuations' energy. The above observations illustrate that most of the nonlinear terms cannot pass through the selective filtering action of the high-gain linear mechanisms in the NSE.

Energy Intensities

Figure 5 shows the captured normal intensities by the resolvent modes for the P4L and P4U solutions. The actual intensities (black curves) are compared with the same quantities obtained using only the most amplified mode pair per Fourier wavenumbers (blue curves) and the five most amplified mode pairs per Fourier wavenumbers (red curves). Notice that the five most amplified mode pairs precisely capture the streamwise energy intensity; cf. figures 5(a) and 5(d). Also note that the most amplified mode pair results in an streamwise intensity that peaks around the constant critical layer where $U(y_c) = c$; cf. figures 5(a), 5(d), 6(a), and 6(c). This is expected since the most amplified resolvent modes are localized around the critical layer (McKeon & Sharma, 2010).

The black curves in figures 5(b), 5(c), 5(e), and 5(f) show that the wall-normal and spanwise intensities are approximately 50 times and 20 times smaller than the streamwise intensities in the P4L and P4U solutions respectively. The blue and red curves show that the mode pairs up to the fifth order cannot fully capture the wall-normal and spanwise intensities. Nevertheless, we show later that the $\overline{uv}$ and mean velocities are reasonably well-captured. The poor representation of $\overline{vv}$ and $\overline{ww}$ can be explained by noting that the resolvent modes are ordered based on the largest amplification of the kinetic energy. Consequently, the mode shapes best represent the streamwise velocity since it contains the largest portion of the energy.

Reynolds Stress and Mean Velocity

The actual mean velocity profile and the mean velocity that the most amplified resolvent modes induce in the flow are compared in figures 6(a) and 6(c) for the P4L and P4U solutions respectively. The solid and dotted black curves respectively show the actual mean velocity and the laminar velocity for the same Re_τ. The captured mean velocity by the most amplified mode pair per Fourier wavenumbers and the five most amplified mode pairs per Fourier wavenumbers are respectively shown by blue and red curves. Notice that the most amplified mode pair captures the departure of the mean velocity from the laminar profile and the higher-order mode pairs further improve the reconstruction of the mean velocity. The mean velocity of the P4L solution is well-captured by the five most amplified mode pairs while the mean velocity of the P4U solution requires higher-order resolvent modes. Figures 5(b) and 5(d) show the streamwise/wall-normal Reynolds stresses. We see that the correlation between wall-normal and streamwise fluctuations is well-captured by the resolvent modes in the P4L solution in spite of poor representation of the wall-normal intensities. This explains accurate reconstruction of the mean velocity by the resolvent modes.

CONCLUSIONS

It was shown that the velocity fluctuations in representative families of fully nonlinear TWS of the NSE can be accurately captured by few most amplified resolvent modes in both pipes and channels. This highlights the integral role of the linear amplification mechanisms in the NSE since the wall-normal shapes of the resolvent modes only depend on the linear mechanisms and the mean velocity of the solution. The phase and amplitude of the modes in the full solution are reflected in the resolvent weights and represent the scaling influence of the nonlinear feedback term $\mathbf{u} \cdot \nabla \mathbf{u}$ that drives the velocity fluctuations.

We showed that even though the nonlinear terms are generally not fully captured by the forcing resolvent modes, the necessary portion of the nonlinear terms from an input-output viewpoint is well-captured. This implies that a relatively small portion of the nonlinear terms can pass through the selective filtering action of the high-gain linear mechanisms in the NSE. This observation can be used to distinguish the 'active' nonlinear terms from the 'inactive' ones and can have significant implications for modeling and control of wall-bounded flows.

It was shown that the large streamwise energy intensities of the considered TWS can be accurately captured by few most amplified resolvent modes per Fourier wavenumbers. The streamwise/wall-normal Reynolds stress and, consequently, the mean velocity are captured reasonably well while the much smaller wall-normal and spanwise energy intensities are poorly captured. This is expected since the resolvent modes are ordered based on the largest amplification of the kinetic energy and, thus, their shapes best represent the streamwise velocity component.

Finally, the low-order synthesized coherent structures from the resolvent model are anticipated to provide viable seeds in the expensive computational search for new exact invariant solutions, thereby reducing the computational cost of such searches.

ACKNOWLEDGEMENT

Support of Air Force Office of Scientific Research under grants FA 9550-09-1-0701 and FA 9550-12-1-0469 (to B.J.M.), FA 9550-11-1-0094 (to M.D.G.), and FA 9550-14-1-0042 (to A.S.S.) is gratefully acknowledged.

REFERENCES

Deguchi, K. & Hall, P. 2014 The high-Reynolds-number asymptotic development of nonlinear equilibrium states in plane Couette flow. *J. Fluid Mech.* **750**, 99–112.

Gibson, J. F., Halcrow, J. & Cvitanović, P. 2008 Visualizing the geometry of state space in plane Couette flow. *J. Fluid Mech.* **611**, 107–130.

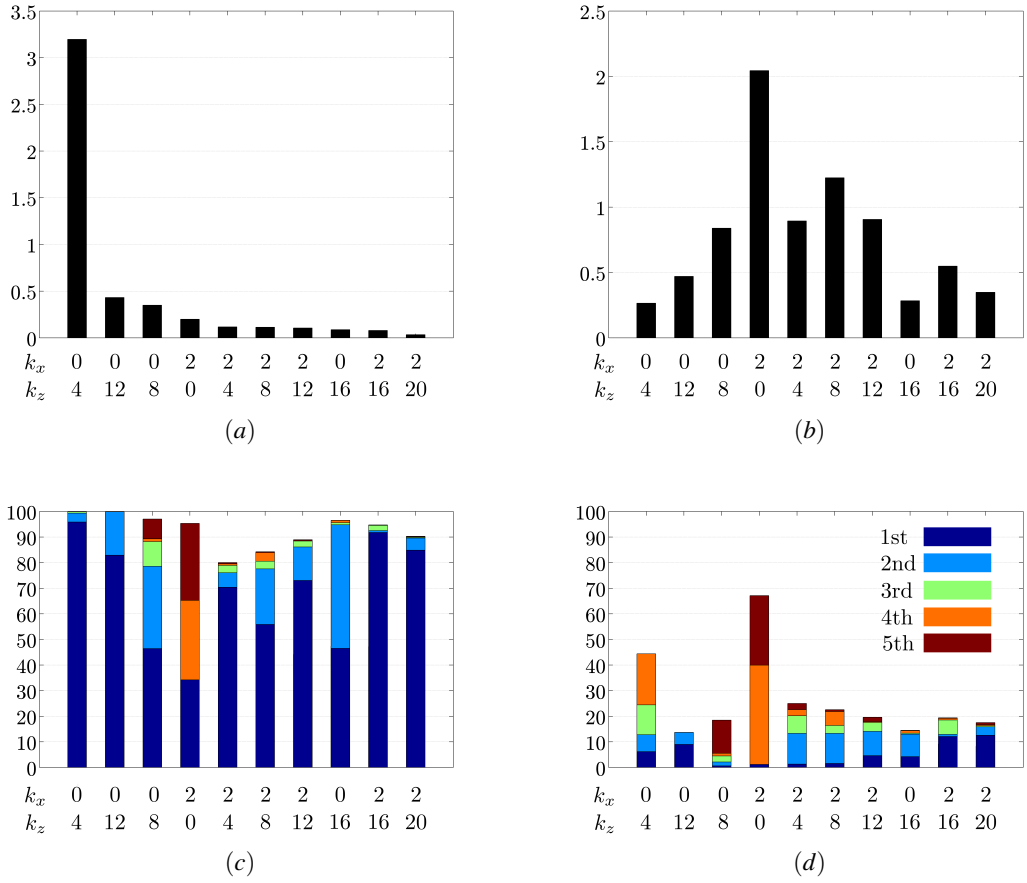

Figure 4. (a) The kinetic energy of the Fourier modes that contain more than 1% of the total energy of fluctuations in the P4L solution with $Re_\tau = 85$ and $c = 25u_\tau$. (b) The L^2 norm of the nonlinear term $\mathbf{u}\cdot\nabla\mathbf{u}$ for the modes shown in (a). (c) The percentage of the kinetic energy of the modes shown in (a) that are captured by the first to fifth pairs of the most amplified resolvent modes. (d) The percentage of the nonlinear terms shown in (b) that are captured by the first to fifth pairs of the most amplified resolvent modes. The legend in (c) is the same as (d). Notice that κ_x and κ_z are normalized with $1/h$.

Hall, P. & Sherwin, S. 2010 Streamwise vortices in shear flows: harbingers of transition and the skeleton of coherent structures. *J. Fluid Mech.* **661**, 178–205.

Li, W., Xi, L. & Graham, M. D. 2006 Nonlinear travelling waves as a framework for understanding turbulent drag reduction. *J. Fluid Mech.* **565**, 353–362.

McKeon, B. J. & Sharma, A. S. 2010 A critical-layer framework for turbulent pipe flow. *J. Fluid Mech.* **658**, 336–382.

McKeon, B. J., Sharma, A. S. & Jacobi, I. 2013 Experimental manipulation of wall turbulence: A systems approach. *Phys. Fluids* **25**, 031301.

Moarref, R., Sharma, A. S., Tropp, J. A. & McKeon, B. J. 2013 Model-based scaling of the streamwise energy density in high-Reynolds number turbulent channels. *J. Fluid Mech.* **734**, 275–316.

Park, J S. & Graham, M. D. 2015 Exact coherent states in Poiseuille flow: connections to Newtonian and viscoelastic turbulent mean profiles. *Submitted* .

Pringle, C. C. T., Duguet, Y. & Kerswell, R. R. 2009 Highly symmetric travelling waves in pipe flow. *Phil. Trans. R. Soc. A* **367** (1888), 457–472.

Sharma, A. S, Moarref, R., McKeon, B. J., Park, J S., Graham, M. D. & Willis, A. P. 2015 Low-dimensional representations of exact coherent states of the Navier-Stokes equations. *arXiv:1503.01701* .

Viswanath, D. 2009 The critical layer in pipe flow at high Reynolds number. *Phil. Trans. R. Soc. A* **367** (1888), 561–576.

Waleffe, F. 2001 Exact coherent structures in channel flow. *J. Fluid Mech.* **435**, 93–102.

Waleffe, F. 2003 Homotopy of exact coherent structures in plane shear flows. *Phys. Fluids* **15**, 1517–1534.

Wedin, H. & Kerswell, R. R. 2004 Exact coherent structures in pipe flow: travelling wave solutions. *J. Fluid Mech.* **508**, 333–371.

Willis, A. P. & Kerswell, R. R. 2008 Coherent structures in localized and global pipe turbulence. *Phys. Rev. Lett.* **100**, 124501.

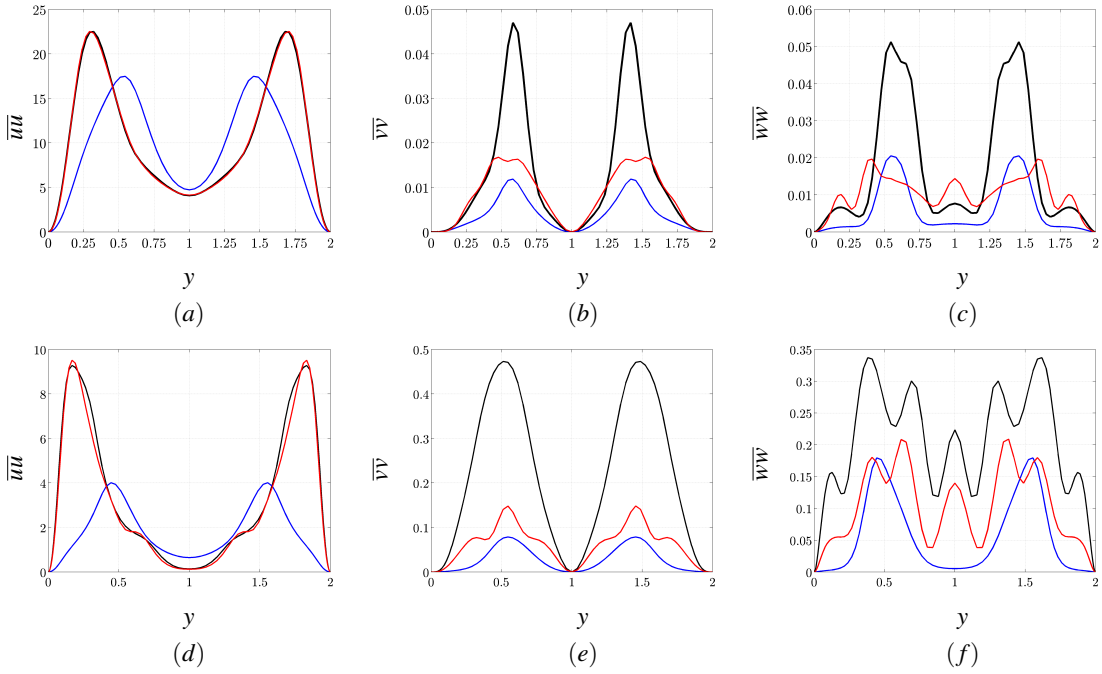

Figure 5. The captured (a,d) streamwise energy intensity (b,e) wall-normal energy intensity and (c,f) spanwise energy intensity by the most amplified pair (blue curves) and the five most amplified pairs (red curves) of resolvent modes in the P4L (top row) and P4U (bottom row) solutions. The actual profiles from numerical simulations are shown in black.

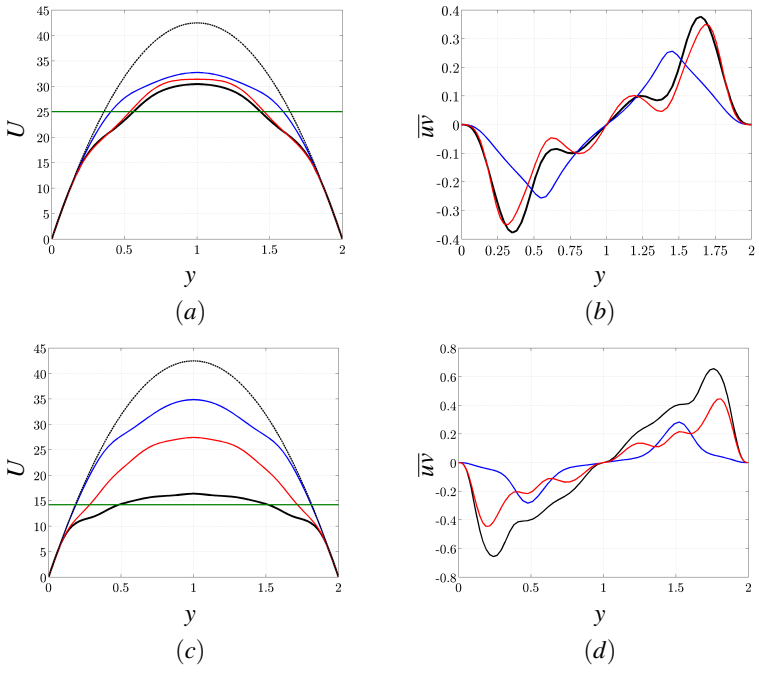

Figure 6. The captured (a,c) mean velocity and (b,d) streamwise/wall-normal Reynolds stress by the most amplified pair (blue curve) and the five most amplified pairs (red curve) of resolvent modes in the P4L (top row) and P4U (bottom row) solutions. The actual profiles from numerical simulations are shown by solid black curves. The laminar profiles are shown by dotted black curves in (a,c). The critical layer where $U(y_c) = c$ occurs at $y_c = 0.55$ for P4L and $y_c = 0.50$ for P4U (green lines).